Supporting information

Highly Efficient Glycolic Acid Electrosynthesis from Waste Ethylene Glycol on Layered Mesoporous Pd_2Ni alloy

Lidan Zhu [a], Juan Chen *[b], Xicheng Lin [a], Yuhang Song [a], Hui Zhao [a], Jiawei Zhang [a], Yuming Dong [a], and Yao Wang *[a]

[a] Key Laboratory of Synthetic and Biological Colloids, Ministry of Education, School of Chemical and Material Engineering, Jiangnan University, Wuxi 214122, China;

Email: wangyao@jiangnan.edu.cn.

[b] Department of Chemistry, Tsinghua University, Beijing, 100084 China.

Email: jchencat163@163.com

Experimental section

Materials. All solvents and reagents were purchased from commercial sources and used as received unless otherwise noted. Sodium tetrachloropalladate (Na_2PdCl_4) was purchased from Shanghai Titan Technology Co., Ltd. Nickelous Nitrate ($Ni(NO_3)_2$), cetyltrimethylammonium bromide (CTAB), 1,3,5-trimethylbenzene (TMB) and Sodium Borohydride ($NaBH_4$) were purchased from China National Pharmaceutical Group Chemical Reagent Co., Ltd. Ethylene glycol (CH_2OHCH_2OH, 99.7%) and Potassium hydroxide (KOH, 99.5%) were purchased from Shanghai Macklin Biochemical Technology Co., Ltd. Ultrapure distilled (18.3 MΩ) was used for all solution preparations. (Methyl sulfoxide)-d6 (DMSO-d6, ≥99.8%) was bought from Shanghai Titan Technology Co., Ltd. 5 wt% Nafion solution was obtained from Alfa Aesar. Ar (99.9%) and oxygen (99.99%) were purchased from Wuxi Xin Xiyi Technology. Pt mesh (0.8 cm × 0.8 cm, 0.5 mm thickness) was ordered from Shanghai Jing Chong Electronic Technology Development Co., Ltd. Glassy carbon electrode and saturated calomel electrode (Hg_2Cl_2/Hg) were purchased from Shanghai Ciyue Industrial Co., Ltd. Zinc-air battery test set and carbon paper matrix were purchased from Changsha Spring New Energy Technology Co., Ltd. Deionized water (Milli-Q) was used for the synthesis. All reagents used as received without further purification.

Catalysis preparation

Synthesis of LM-Pd_xNi. Pd_xNi electrocatalysts with a layered stacked morphology (denoted as LM-Pd_xNi) with varying Pd contents were synthesized via a facile solution-phase route, using Na_2PdCl_4 and $Ni(NO_3)_2$ as metal precursors, cetyltrimethylammonium bromide (CTAB) as a mesoporous template, 1,3,5-trimethylbenzene (TMB) as a structure-directing agent, and $NaBH_4$ as a reducing agent. Typically, 200 mg of CTAB was dissolved in 40 mL of water at room temperature. Then, 200 μL of TMB was added to the above solution. After stirring for 20 min, 500 μL of aqueous solution containing 25 mg of Na_2PdCl_4 and 250 μL of aqueous solution containing 8.7 mg of $Ni(NO_3)_2$ were introduced. Following further stirring for 30 min, 1.5 mL of a freshly prepared solution containing 12.6 mg of $NaBH_4$ was injected into the mixture. The reaction was carried out at 90 °C for 1.5 h to yield the product (LM-Pd_2Ni). Subsequently, the mesoporous template and structure-directing agent were removed by repeated washing with water/ethanol to expose clean metallic sites within the mesopores. Similarly, LM-Pd_xNi samples with different Pd loadings were prepared by the same procedure but varying the amount of Na_2PdCl_4.

Synthesis of LM-Pd. The LM-Pd was prepared by a similar procedure as preparing LM-Pd_xNi but without the addition of $Ni(NO_3)_2$.

Catalysts characterization. X-ray diffraction (XRD) analysis was carried out on a Bruker D8 focus diffraction spectrometer using Cu Kα radiation with a scanning angle (2 theta) of 20~90^0 at a speed of 5^0 min^{-1}, operated at 40 kV and 40 mA. Energy dispersive X-ray spectroscopy (EDS) was carried out using 4 in-column Super-X detectors. X-ray photoelectron spectra (XPS) were carried out on a Thermo ESCALAB 250Xi spectrometer using Al-Kα radiation source. The binding energies were calibrated using C_{1s} peak of contaminant carbon (Binding Energy = 284.8 eV) as an internal standard. Transmission electron microscopy (TEM) images of samples were obtained to characterize the sizes and morphologies of on a Hitachi H-800 TEM.

Electrode preparation. To prepare the Anode electrode, catalyst ink that containing 1~2 mg of as-crafted catalyst, 500 μL of ethanol, 250 μL of Deionized water solution was sonicated for 30 min. The catalyst ink was then loaded onto a glassy carbon electrode, and dried at room temperature.

Evaluation of EGOR performance. All electrochemical measurements were performed in a single-port electrolytic cell, a glassy carbon electrode, a saturated calomel electrode and a platinum cathode. The electrolysis was controlled by CS (CS310H, Wuhan Corrtest Instruments Corp., Ltd) electrochemical workstation. Ag/AgCl was used as the reference electrode and it was calibrated with respect to RHE: E (RHE) = E (Hg_2Cl_2/Hg) + 0.0592 × PH + 0.241. All the electrocatalytic reactions were conducted at ambient pressure and temperature.

To gain the electrochemical active surface areas (ECSAs), specific activities and mass activities of catalysts, cyclic voltammetry (CV) tests were performed in Ar- saturated 1.0 M KOH and Ar-saturated 1.0 M KOH and 1.0 M EG at a scan rate of 50 mV s^{-1}, respectively. For the kinetic measurements, CV curves were collected in Ar-saturated 1.0 M KOH and 1.0 M EG. The chronoamperometry curves of the catalysts were tested in Ar-saturated 1.0 M KOH and 1.0 M EG for 2000 s at the potential of 0.75 V (vs RHE) different scan rates (20 mV-80mV). To obtain CO stripping curves, the catalysts electrode was first scanned in 1.0 M KOH solution and purged with CO at 0.15 V for 30 min to cover the surface with CO. Then, the electrode was transferred into another 1.0 M KOH solution for CO stripping measurements in the potential range between -1.07 V and 0.17 V.

Electrooxidation products analysis. The liquid products in anode chambers were collected during electrolysis and analyzed by ^{1}H NMR spectroscopy (Advance III HD 400 MHz, Bruker), after diluting 0.5 mL of electrolyte solution three times with deionized water, 0.5 mL was taken and mixed with 0.1 mL of DMSO (internal standard, diluted to 25 ppm (v/v) by deuterated water).

The corresponding faraday efficiency (FE) toward formate and glycolate are calculated based on the following equations:

$$FE_{formate} = 100\ \% * C_{formate} * V * n * F / Q_{total} \text{ and } FE_{glycolate} = 100\ \% * C_{glycolate} * V * n * F / Q_{total}$$

Where $C_{formate}$ and $C_{glycolate}$ correspond to the respective concentrations; V is the volume of solution; F is Faraday constant (96485 C/mol); n is the number of electron transfer for each product formation, n = 3 for formate and n = 4 for glycolate; Q_{total} is the integration of the i-t response curve (chronoamperometry), representing the total charge transfer.

The selectivity of formate is calculated by the following equation:

$$Selectivity_{formate} = 100\ \% * C_{formate} / (C_{formate} + C_{glycolate}).$$

In-situ ATR-SEIRAS measurement. The in-situ attenuated total reflection-surface-enhanced IR absorption spectroscopy (ATR-SEIRAS) spectroscopy experiments were conducted in a modified electrochemical cell that integrated into a Nicolet iS50 FT-IR spectrometer equipped with mercury-cadmium-telluride (MCT) detector cooled by liquid nitrogen. The preparation of the working electrode is divided into two steps. In the first step, an Au thin film is chemically deposited on the surface of the hemispherical silicon crystal. The Au-coated Si crystal was used as the substrate to conduct electrons and the element to enhance the infrared signal. Cyclic voltammetry test was carried out on silicon crystal loaded with Au film with 0.1 M $HClO_4$ as the electrolyte at a scan rate of 100 mV s^{-1} until a repeatable cyclic voltammetry curve was obtained. Then, the catalyst ink (10 mg catalyst, 1 mL ethanol and 50 μL Nafion) was dropped onto the Au film with the loading of 0.1 mg cm^{-2}. The working electrode was mounted in a three-electrode electrochemical cell, where a platinum sheet and an Hg_2Cl_2/Hg electrode served as the counter and reference electrodes, respectively. Before performing in situ ATR-SEIRAS, 1M KOH+1M EG electrolyte was bubbled with Ar for 30 min until saturated. The FTIR chamber and light path were continuously purified with Ar at about 6 L min^{-1} and 1 L min^{-1}, respectively. All spectra

are expressed in absorbance unit as $-\log(I/I_0)$, with I and I_0 representing the sample and reference spectra, respectively. The spectral resolution was 8 cm^{-1} for all the measurements. Each spectrum is the superposition of 32 interferograms, and the acquisition period is 25 s per spectrum.

DFT calculations. In this work, all the calculations were performed in the Vienna ab initio simulation package (VASP) by DFT-D3 method. [1] Interactions between the valence electrons and ionic cores were described by projector augmented wave (PAW), [2] and the generalized gradient approximation (GGA) with Perdew-Burke-Ernzerhof (PBE) functional [3] was applied to calculate exchange-correlation energies. The Monkhorst-Pack grid is 1×1×1 to perform the Brillouin-zone integrations. The energy cutoff of 450 eV was used to the plane-wave basis set. The Pd (1 1 1) surface was constructed as the research model, and the LM-PdNi model was built by replacing a surface Pd atom with a Ni atom. The top two layers were relaxed and other atoms were fixed during all the optimization process. The convergence criterion is 1×10-5 eV for energy and 1×10-4 eV/Å for force. In addition, the transition states were searched by combing nudged elastic band (NEB) method [4] and dimer method, [5] the transition states were proved by imaginary frequency.

1. Grimme, S.; Antony, J.; Ehrlich, S.; Krieg, H. J. Chem. Phys. 2010, 132, 154104.

2. Kresse; Joubert, D. From Ultrasoft Pseudopotentials to the Projector Augmented-Wave Method. Phys. Rev. B: Condens. Matter Mater. Phys. 1999, 59, 1758-1775.

3. Perdew, J. P.; Burke, K.; Ernzerhof, M. Generalized Gradient Approximation Made Simple. Phys. Rev. Lett. 1996, 77, 3865-3868.

4. Henkelman, G.; Uberuaga, B. P.; Jonsson, H. J. Chem. Phys. 2000, 113, 9901-9904.

5. Henkelman, G.; Jonsson, H. J. Chem. Phys. 1999, 111, 7010-7022.

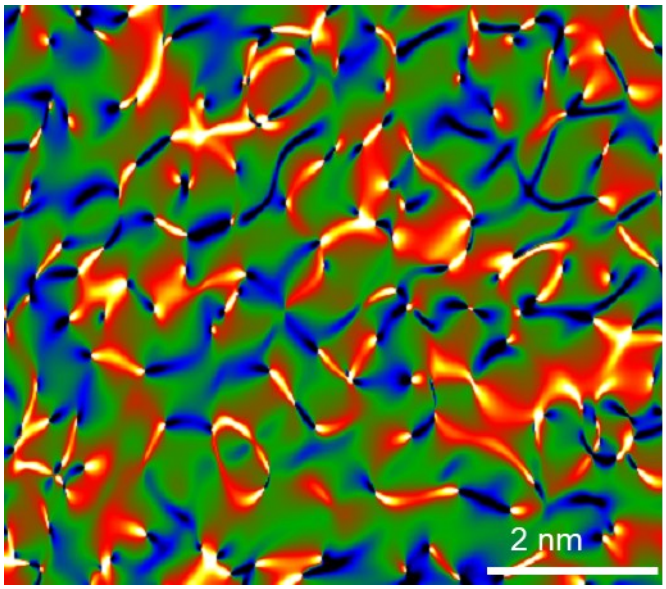

Figure S1. Lattice strain (ε_{xx}) measured from GPA of HRTEM images for LM-Pd_2Ni alloy.

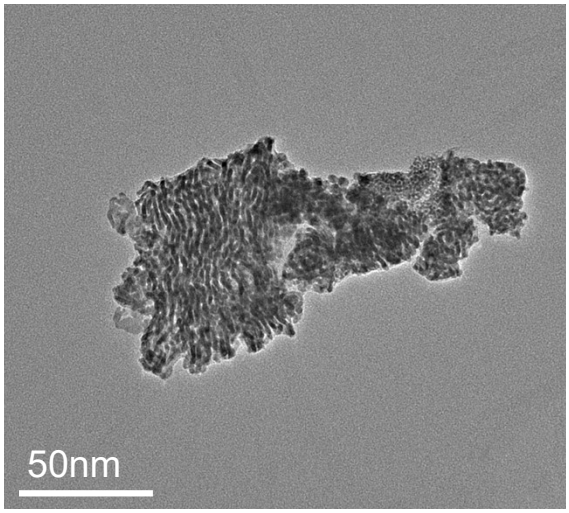

Figure S2. TEM image of LM-Pd.

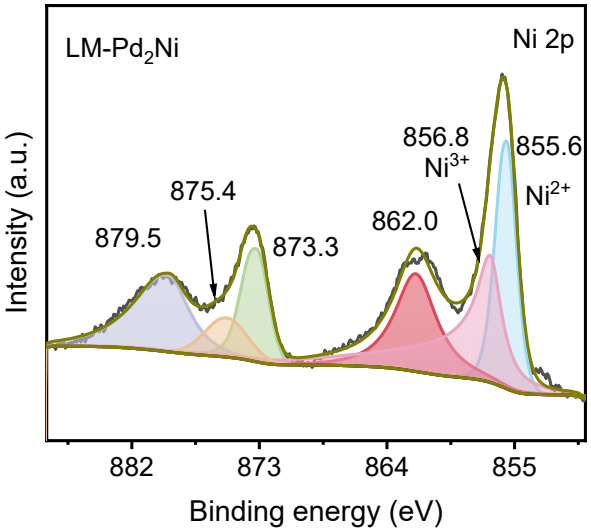

Figure S3. Ni 2p XPS spectra of LM-Pd_2Ni.

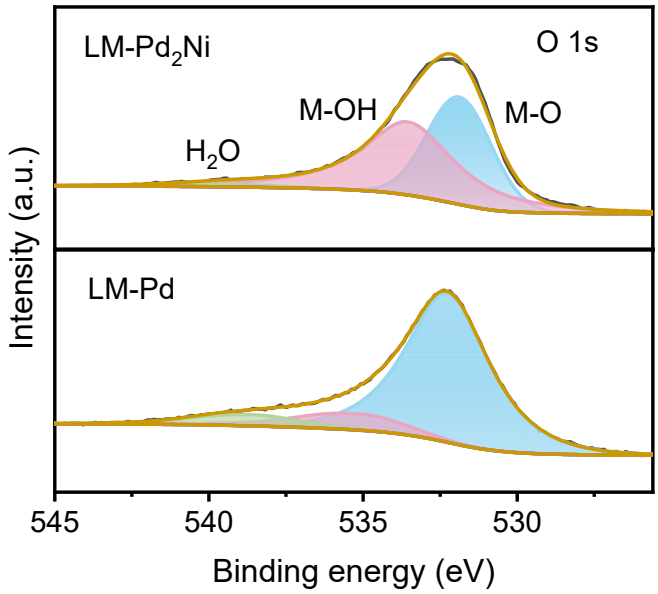

Figure S4. O 3d XPS spectra of LM-Pd_2Ni and LM-Pd.

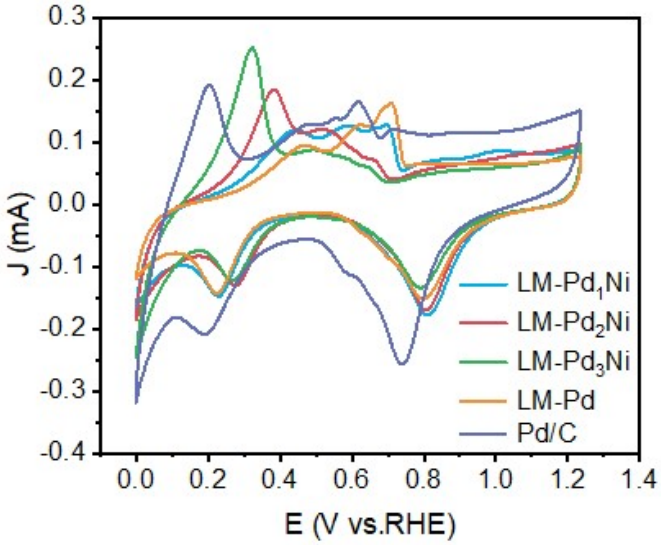

Figure S5. Cyclic–voltammogram curves in 1M KOH of LM-PdNi, LM-Pd and Pd/C.

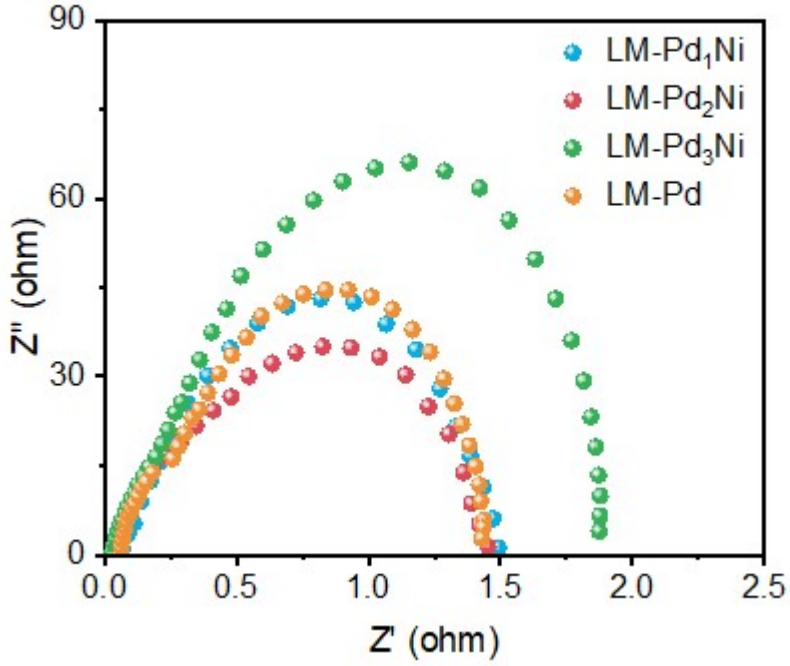

Figure S6. EIS curves of in 1M KOH of LM-PdNi, and LM-Pd.

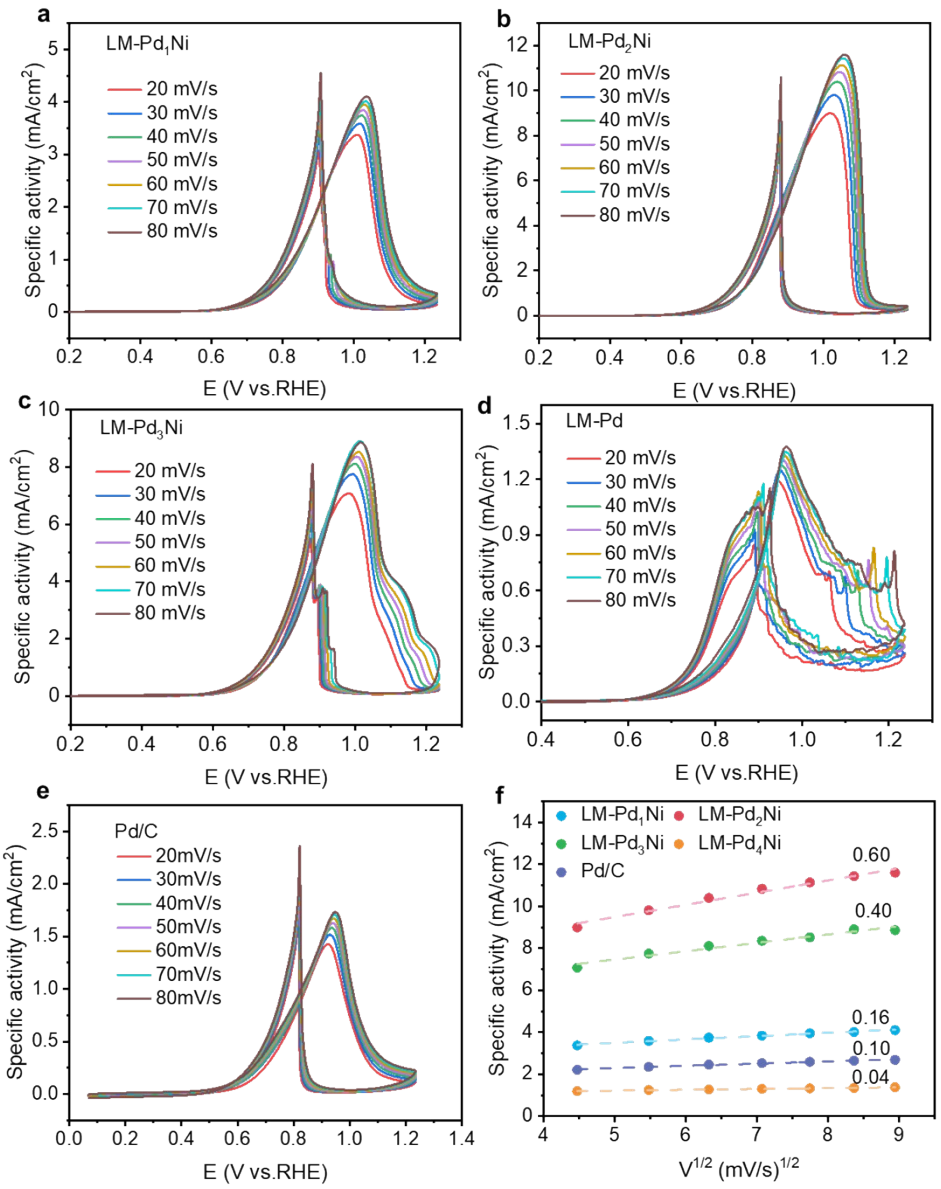

Figure S7. CV curves at different scan rates from 20 to 80 mV s^{-1} for (a) LM-Pd_1Ni, (b) LM-Pd_2Ni, (c) LM-Pd_3Ni, (d) LM-Pd and (e) Pd/C. (f) The plots of forward peak current J (mA/cm^2) vs. the square root of the scan rate ($v^{1/2}$) for EGOR.

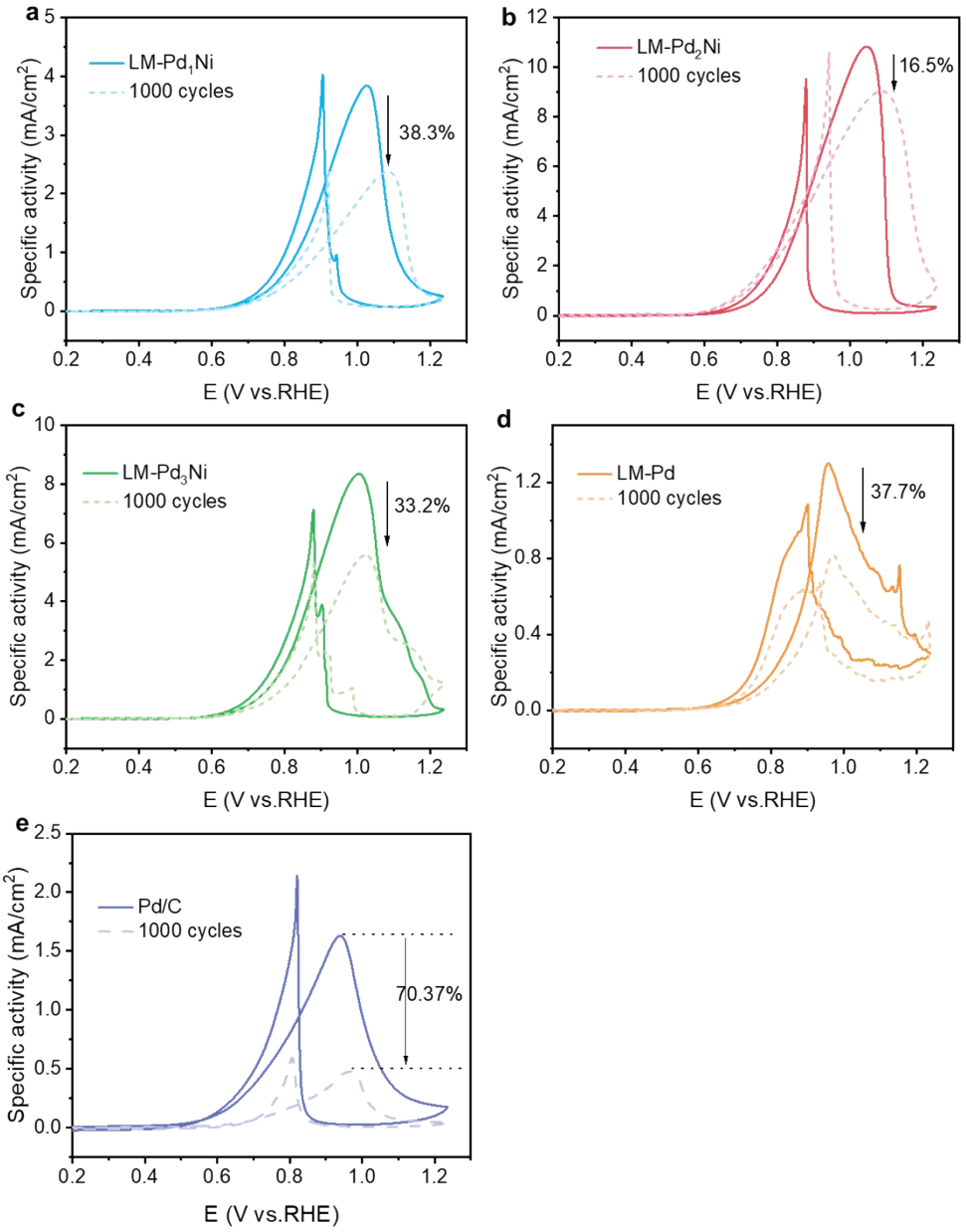

Figure S8. The CV curves of EGOR before and after reaction for (a) LM-Pd_1Ni, (b) LM-Pd_2Ni, (c) LM-Pd_3Ni, (d) LM-Pd and (e) Pd/C.

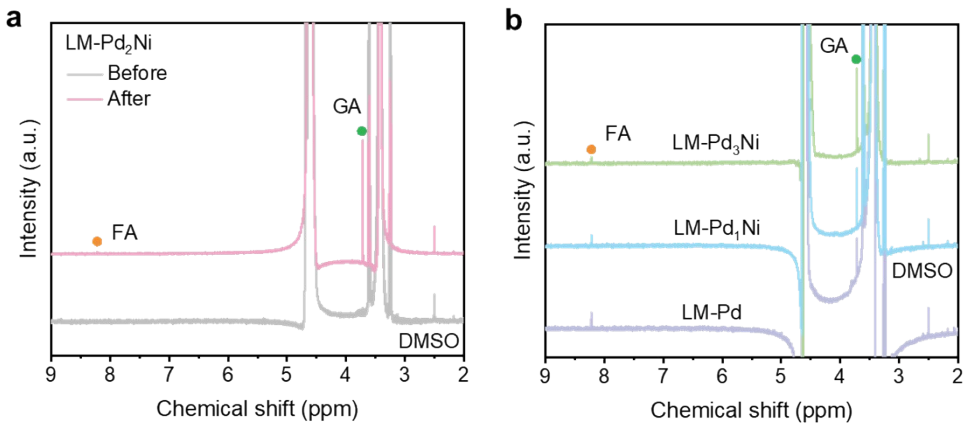

Figure S9. [1]HNMR spectrum of EGOR before and after reaction on LM-Pd, LM-Pd_1Ni, LM-Pd_2Ni and LM-Pd_3Ni.

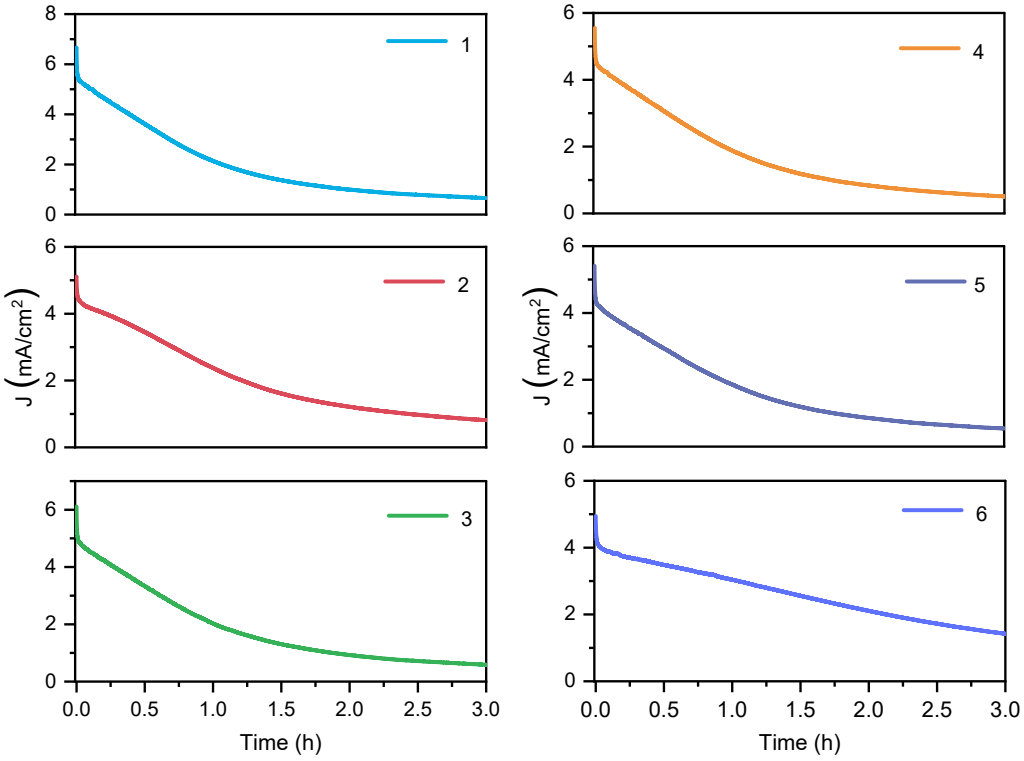

Figure S10. I-t tests of EGOR for LM-Pd_2Ni.

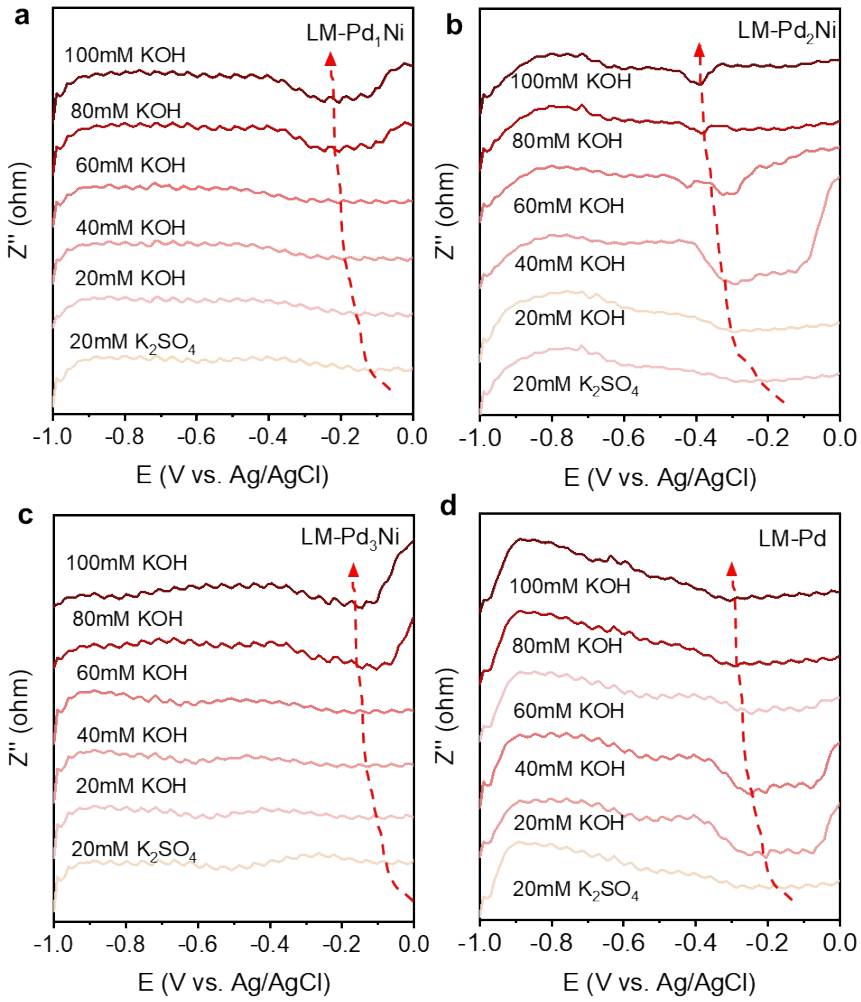

Figure S11. The electrochemical impedance-potential spectra of (a) LM-Pd_1Ni, (b) LM-Pd_2Ni, (c) LM-Pd_3Ni, (d) LM-Pd in 0 20, 40, 60, 80 and 100 mM KOH solutions, respectively.

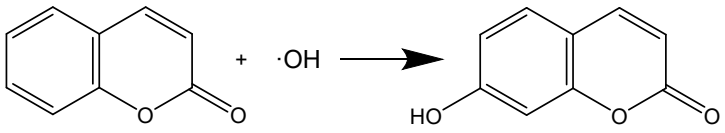

Figure S12. Reaction equation ·OH and coumarin.

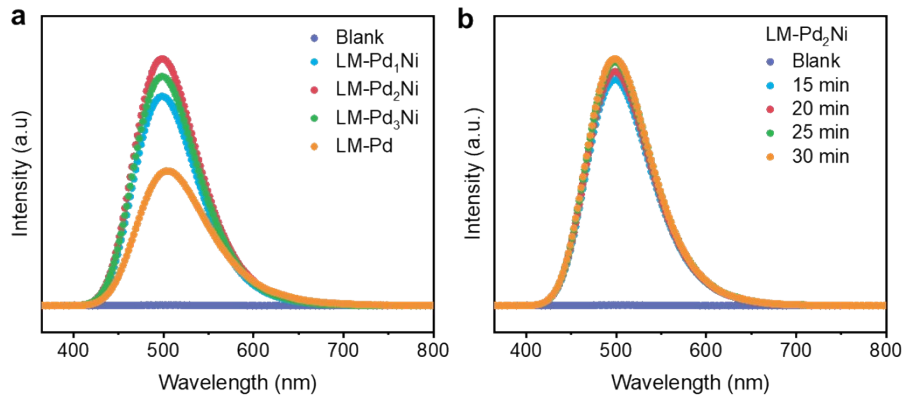

Figure 13. (a) Fluorescence spectra for the detected free *OH in electrolyte using a coumarin (0.2 mm) indicator with the excitation wavelength of 350 nm. (b) Fluorescence spectra for the detected free *OH in electrolyte using a coumarin (0.2 mm) indicator with the excitation wavelength of 350 nm for different reaction time of LM-Pd_2Ni.

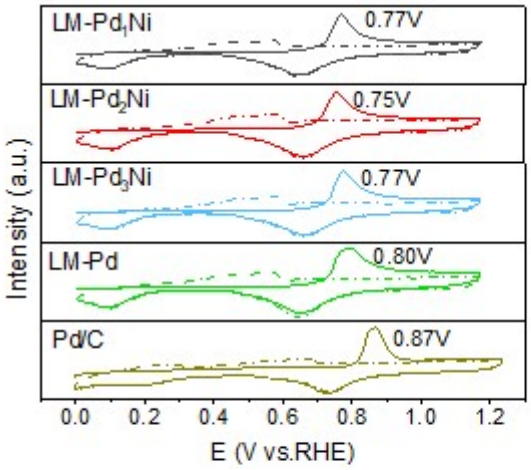

Figure 14. CO stripping experiments of LM-Pd_2Ni, LM-Pd and Pd/C.

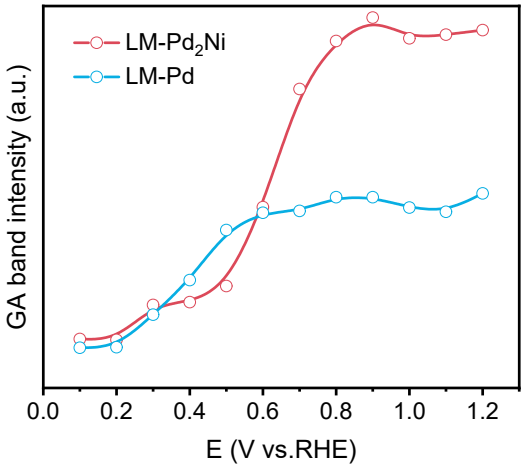

Figure 15. The band intensity of GA under different potentials for LM-Pd_2Ni and LM-Pd.

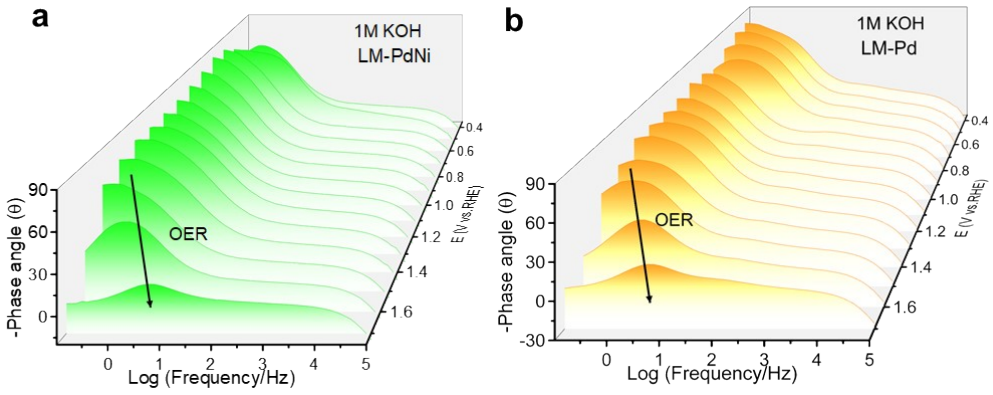

Figure S16. Bode-phase plots of (a) LM-Pd_2Ni and (b) LM-Pd in 1 M KOH under different potentials.

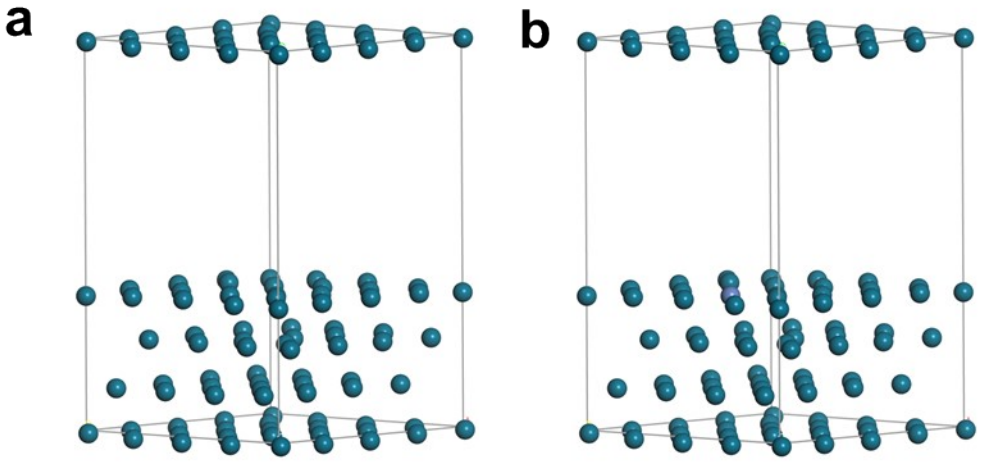

Figure S17. Calculation models of LM-Pd and LM-PdNi.

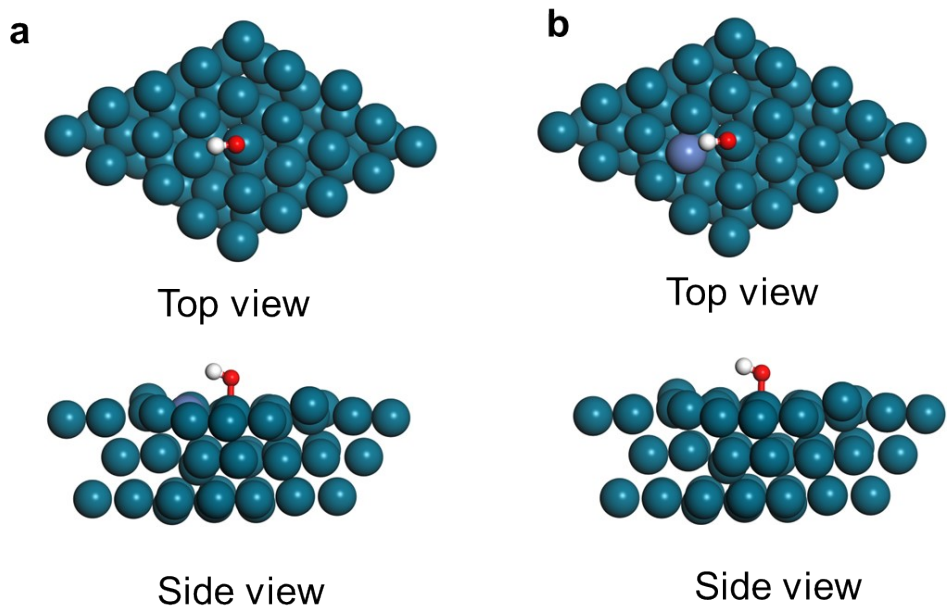

Figure S18. The model configurations of the *OH on (a) LM-Pd and (b) LM-PdNi.

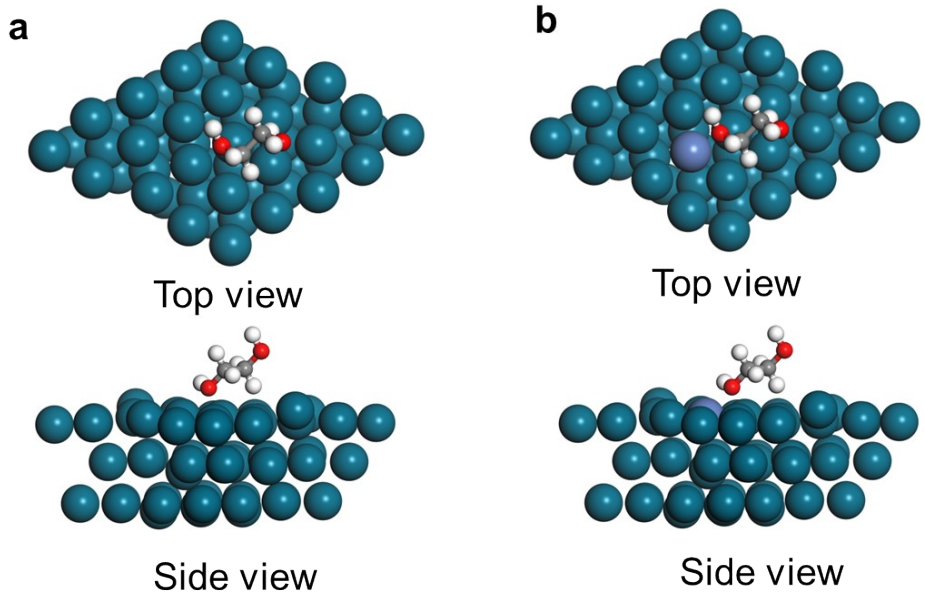

Figure S19. The model configurations of the *EG on (a) LM-Pd and (b) LM-PdNi.

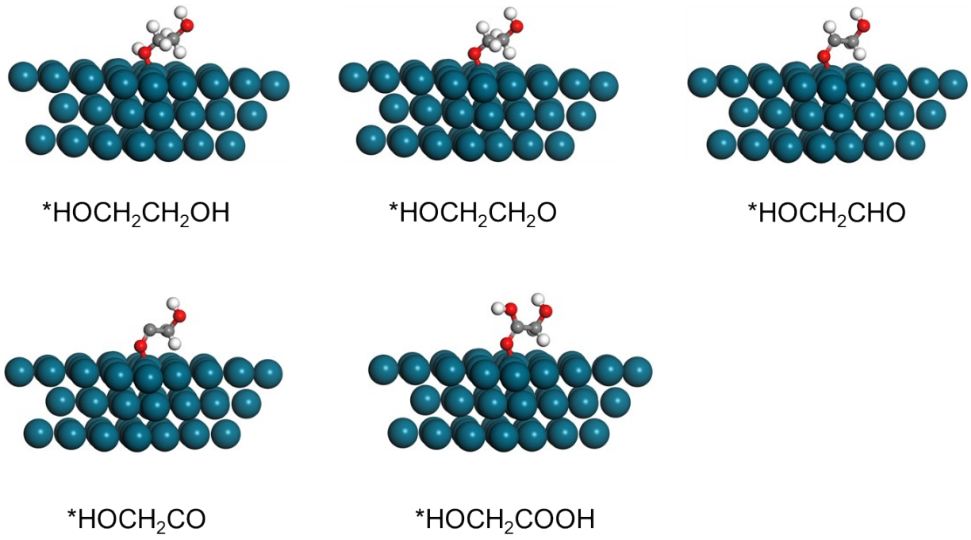

Figure S20. The model configurations of the EG oxidation process on LM-Pd.

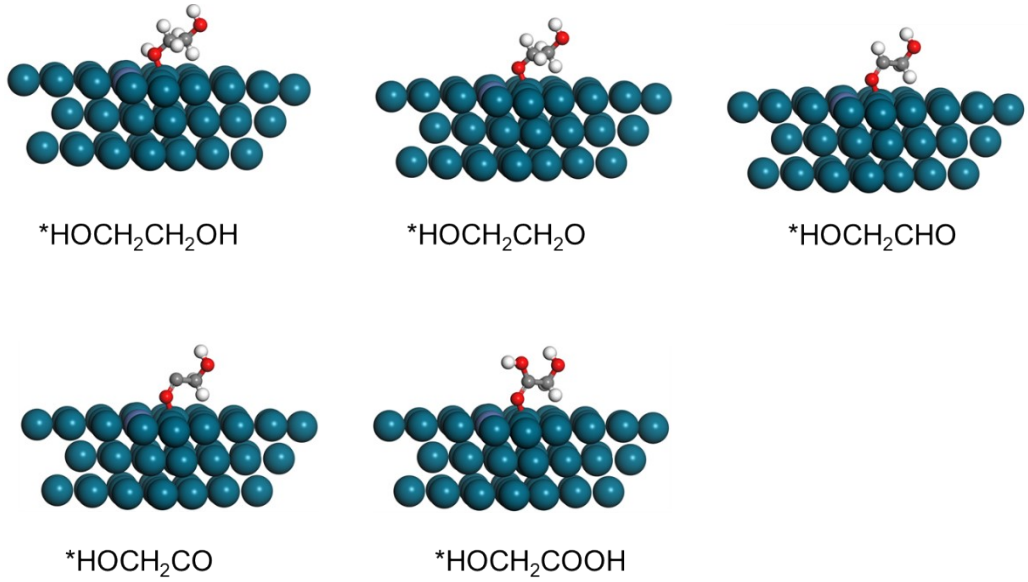

Figure S21. The model configurations of the EG oxidation process on LM-PdNi.

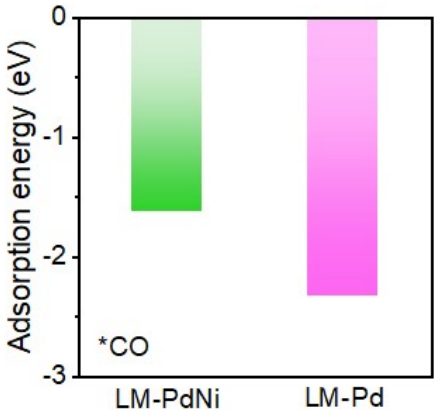

Figure S22. Adsorption energy of *CO on LM-Pd and LM-PdNi.

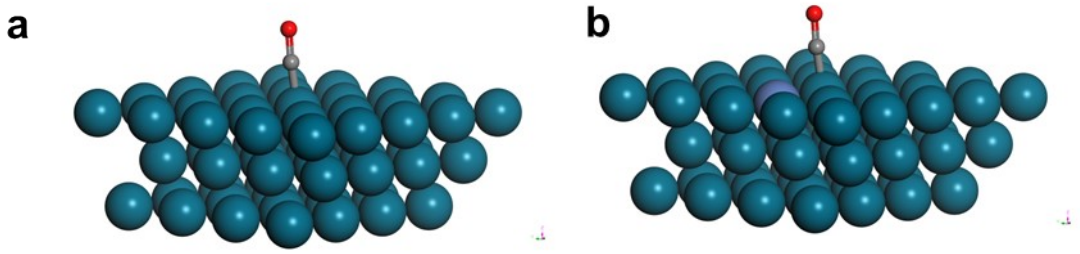

Figure S23. The model configurations of the *CO adsorption on (a) LM-Pd and (b) LM-PdNi.